Automated Marker Localization in the Planning Phase of Robotic Neurosurgery

Suligoj, Filip; Svaco, Marko; Jerbic, Bojan; Sekoranja, Bojan; Vidakovic, Josip

IEEE Access
Multidisciplinary | Rapid Review | Open Access Journal

Received May 12, 2017, accepted June 15, 2017, date of publication June 22, 2017, date of current version July 24, 2017.

Digital Object Identifier 10.1109/ACCESS.2017.2718621

Automated Marker Localization in the Planning Phase of Robotic Neurosurgery

FILIP ŠULIGOJ, MARKO ŠVACO, BOJAN JERBIĆ, BOJAN ŠEKORANJA, AND JOSIP VIDAKOVIĆ
Department of Robotics and Production System Automation, Faculty of Mechanical Engineering and Naval Architecture, University of Zagreb, Zagreb 10002, Croatia

Corresponding author: Filip Šuligoj (filip.suligoj@fsb.hr)

This work was supported by the Croatian Scientific Foundation through the Research Project ACRON under Grant HRZZ-4192.

ABSTRACT Accurate patient registration is a critical issue in medical image-guided interventions. The neurosurgical robotic system RObotic Neuro-NAvigation (RONNA) uses four retro-reflective spheres, on a marker attached to the patient's cranial bone, for patient registration in physical and image space. In this paper, the algorithm for automatic localization of spherical fiducials in CT scans is presented and clinically evaluated. The developed localization algorithm uses a unique approach, which combines machine vision algorithms, biomedical image filtration methods, and mathematical estimation methods. The performance of the localization algorithm was evaluated in comparison with four skilled human operators. The measurements were based on twelve patient and eight lab phantom CT scans. The localization error of the algorithm in comparison with the human readings was smaller by 49.29% according to the ground truth estimation and by 45.91% according to the intra-modal estimation. Localization processing time was reduced by 84.96%. Reliability in terms of successful localization of the fiducial marker was 100% for 20 different test samples containing a total of 116 spherical fiducials. Based on the tests carried out in clinical conditions, the localization algorithm has demonstrated reliability with a high degree of accuracy and short processing time. The developed algorithm provides fully automated and accurate machine vision-based patient localization for the neurosurgical clinical application of the robotic system RONNA.

INDEX TERMS Accuracy, biomedical image processing, clinical trials, DICOM, medical robotics, stereotaxy.

I. INTRODUCTION

Medical image-guided interventions (IGI) use information acquired from preoperative imaging methods such as computed tomography (CT) and magnetic resonance imaging (MRI). Three-dimensional (3D) volume is reconstructed from two-dimensional (2D) slices in visualization software and is then used for preoperative planning, accurate surgical tool guidance, and surgery target visualization. These methods have been introduced into clinical applications such as neurosurgery, cardiac surgery, orthopaedic surgery, and others [1]. For example, neuronavigation systems are commonly used in clinical practice to guide the neurosurgeon's instrument inside the cranial space or vertebral column. A general sequence of steps in medical IGIs includes: a preoperative scan obtained from a CT or an MRI scanner; preoperative visualization and intervention planning; patient-to-image registration; surgical tool guidance and intraoperative visualization. A surgeon uses the images acquired in the preoperative phase for visualizing and planning of surgery targets. In machine vision, the term "registration" implies the aligning of two images of the same environment or object, which can be taken from different viewpoints, with different devices, and at different times [2]. A process of registration in the context of medical image registration and IGI implies the determination of a spatial transformation between the image and patient coordinate systems [3], [4]. Surgery points determined in preoperative planning can be targeted in the physical space only after the image space and the physical space have been aligned. In general, fiducial marker localization is the process of determining the exact marker coordinates in the image space and the physical space. Fiducial points located on the fiducial marker are used as references in the registration process.

The proportion of misalignment in registration reduces the accuracy of the surgical tool positioning to the planned target. Steinmeier *et al.* [5] used two different medical neuronav-

igation systems with a plexiglass phantom for testing the influence of different factors on the tool positioning accuracy. Their conclusion was that the accuracy of neuronavigation systems greatly depends on the registration procedure. The dependence of neuronavigation accuracy on different parameters such as slice thickness, the field of view, and type of sequences for CT and MRI is measured in [6]. In that study, CT procedures proved to be more accurate than MRI.

Another factor influencing the registration accuracy is the type of marker used for the patient localization. Registration methods in IGI with regard to the type of marker [7] are extrinsic, intrinsic, and non-image based (calibrated coordinate systems). Extrinsic methods rely on attaching external objects to a patient prior to imaging. External objects used in medical procedures are stereotactic frames, rigid bone- attached markers, other externally attached frames, and adhesive markers. Improved marker insertion methods and benefits of bone-implanted markers have been demonstrated in [8] and [9]. Advantages of extrinsic methods in terms of accuracy in comparison with the intrinsic and calibration-based methods are identified and evaluated in [10]. In the study, seven different modes of patient registrations were compared based on in vivo measurements including thirty patients. Bone-attached markers provide the highest degree of the application and the targeting accuracy when used in IGI.

Methods used in IGI enable the practical use of robots in situations where an accurate robot- guided surgical tool is needed. From the robotics point of view, many problems in neurosurgery can be classified as rigid body transformations and hence the implementation of robot systems in neurosurgery is suitable. Growth trends in robotic neurosurgery presented in [11] and [12] are sure to continue because of the proven capabilities of robot systems such as accuracy, repeatability, tremor-less movement, and automation of surgery procedures. The accuracy of surgical robot systems is of the utmost importance when evaluating the plausibility of implementation in different medical procedures. A higher degree of the system accuracy enables us to implement it in even more demanding medical procedures.

Our research group has developed a robotic system for neurosurgical applications, RONNA. In the current development stage, the prototype is included in a series of human clinical applications in cooperation with a team of neurosurgeons from the Clinical hospital Dubrava. RONNA is composed of two industrial robot arms used for the navigation and precise guidance of surgical tools. The main system components of RONNA, the operating flow chart of the operating procedure, and a novel visual calibration method are presented in [13] and [14]. In the registration procedure, a bone-implanted marker carrying four spherical fiducials must be localized in both the CT scan and the robot coordinate system in the physical space. The bone-implanted marker is used to provide safe positioning. In our recent study [15], a low-cost lightweight industrial robot arm guided with a medically certified optical tracking system was navigated to positions manually localized by the human operator from a CT scan. The purpose of the study was to measure the main accuracy categories of the system and to assess whether the optical tracking system could improve the positioning accuracy of the robot tool. The combined root mean square (RMS) error of the human operator and the CT scanner was measured at 0.462 mm for a calibration board.It was concluded that one of the main factors contributing to the imaging and the registration error was the manual localization of features in the CT scan.

The main disadvantages of manual localization are: localization duration, the possibility of human error, and insufficient accuracy. In the RONNA surgery procedure, manual localization must be conducted after the patient with the attached fiducial marker has been scanned and taken to the operating room. The operator visually determines the centre of every spherical fiducial in the exact order as the coordinate system has been defined. Since the neurosurgeon can only start with the target planning after the localization procedure, it is crucial that this phase takes as little time as possible. Consequently, this puts additional pressure on the human operator.

In this paper, we present a novel algorithm for accurate localization of fiducial markers in the image space (CT scans). The drawbacks of manual localization are overcome by means of machine vision algorithms. An extrinsic, bone-implanted fiducial marker with four retro-reflective spherical fiducials is used for localization. Circular Hough Transform (CHT)-based algorithm is used for finding all the potential circles in two orthogonal image projections (axial and sagittal). Due to the visually cluttered environment in 2D CT images, many false positive circles are detected. An iterative clustering method is developed for circle grouping. Verified clusters are used for the calculation of sphere centres. Euclidean distance filters are used in the clustering phase and for the elimination of potential false positive results. Two methods for estimating spherical fiducial centres from the detected clusters are implemented: RANSAC Linefit and Spherefit. Robustness, accuracy, reliability, and processing time of the algorithm for the automated localization of fiducial markers are verified in the conducted clinical trials. The degrees of accuracy of the automated algorithm and the manual localization conducted by trained operators are compared with ground truth and intra-modal measurements.

II. RELATED WORK

Methods for the localization of fiducials in volumetric images can be manual, semi-automatic, and automatic. Manual localization is a general approach that involves human operators and that is used with different fiducial types and imaging technologies. Semi-automatic and automatic localization algorithms have been introduced to overcome previously stated drawbacks of manual localization and to improve localization and registration accuracy results. A priori knowledge such as physical features and intensity values of the marker are often used for the localization of fiducial points.

An example of semi-automatic fiducial localization is presented in [16]. First, the operator designates the rough location of the fiducials and then the algorithm localizes the fiducial points accurately using the intensity-based registration with mutual information similarity measure. As the authors point out, the advantage of such an approach is that it can be used for different types of fiducials and with different imaging modalities. Gerber *et al.* [17] have developed a registration system for robotic microsurgery that localises the fiducial screw in both the physical and the image space. Both methods use the semi-automatic approach for the coarse localization of the screw. Fiducial localization uses cropped sub-volumes of the image. Sub-volumes are selected by the operator and fitted to the 3D surface model of the screw. The robot uses a force-torque sensor for precise localization of the screw head in the physical space.

An automatic knowledge-based technique for localizing the centroids of cylindrical markers externally attached to the patient's head in the CT and the MR image volumes is presented in [18]. Machine vision algorithms are used to find the markers whose voxel intensities are higher than those of the surrounding space. Similarly to our research, Yaniv [19], [20] uses externally placed spherical fiducials for localization. When using a c-arm-based cone-beam CT (CBCT) instead of the localization in volumetric images, the developed method is able to provide coordinates of the fiducials from the projection images. The related research [21] proposes a 3-D surface modelling approach for the localization of spherical radio-opaque markers in CT scans. In that case, the optimized algorithm parameters deliver sub-millimeter localization accuracy with different CT resolutions. Performance of a block matching-based automatic registration algorithm is tested by Isambert *et al.* [22]. The accuracy of the process was measured for two different phantoms on CT, MR and positron emission tomography (PET) images. The block matching-based algorithm yielded the below voxel accuracy. In a pilot study [23], the patient's teeth were successfully used in marker-less registration. The system displayed high accuracy in the real-time 3D image matching of stereo vision data and integral videography image derived from a CT scan.

Fiducial localization in volumetric images is an essential requirement in robot-assisted neurosurgical procedures. Non-invasive markers are preferred for their simpler mounting procedure but they show lower accuracy. For example, the stereotactic robot system Rosa is used in intracranial procedures [24]. Lefranc *et al.* [25] assess the impact of imaging modality, registration method, and intraoperative flat-panel computed tomography on the application accuracy of the ROSA stereotactic robot. Their measurements show that the frame-based stereotactic registration in robotic surgery is more accurate than the frameless registration. In vitro testing of the Neuromate neurosurgical robot showed similar results regarding the impact of registration method on the application accuracy. In vitro testing [26] showed the application accuracy of the frame-based localization system to be 0.86 ± 0.32 mm and 1.95 ± 0.44 mm of the frameless localization system. In a more recent study [27], in vitro and in vivo tests carried out with the Neuromate's frame-based application showed improved accuracy.

III. MATERIALS AND METHODS

For testing the reliability and accuracy of the developed localization algorithm, we used: a bone-attached fiducial marker developed for the RONNA system, a Siemens Sensation 16 CT scanner, and the Medinria medical imaging software. A Ferranti Merlin 750 coordinate measuring machine (CMM) was used for ground truth (GT) measurements of the test phantom. The declared expanded measuring uncertainty of the CMM is equal to $4 + 4 \times \mathrm{L}\ \mu$m, for L being the distance measured in metres. The testing procedure was conducted as a part of the standard clinical procedure for stereotactic neurosurgery where the marker was fixed on the patient and on the test phantom. An aluminium marker with four retro-reflective spheres attached to a patient and the test phantom is shown in Fig. 1 and Fig. 2.

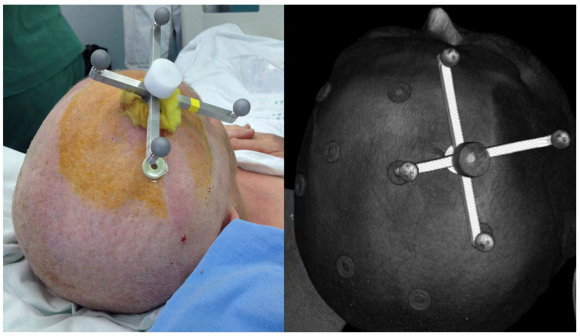

FIGURE 1. Patient with a bone-attached fiducial marker.

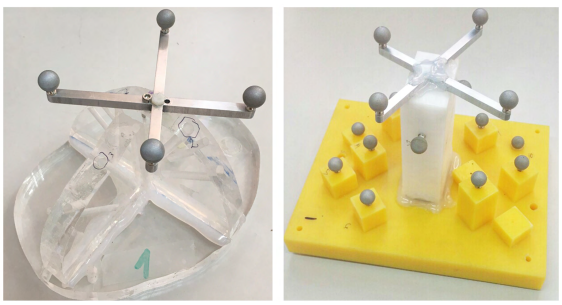

FIGURE 2. Test phantoms with an attached fiducial marker.

Retro-reflective spheres, i.e. spherical fiducials (fiducial points) are localized both in the physical and the image space. Infrared cameras are used for robot localization in the physical space and the developed automatic localization algorithm is used for localization in the image space. Spatial positioning of the fiducial spheres on the fiducial marker gives a unique distance between any two spheres. The first test phantom shown in Fig. 2 (left) was made of several (methyl methacry-

late) oval plates attached to each other. The volume and the shape of the test phantom are made to resemble a human head.

The second test phantom shown if Fig.2 (right) was equipped with the fiducial marker and additional twelve retro-reflective spheres that were used as target points. The fiducial marker was placed on the test phantoms in a similar way to the fiducial marker on the patient head.

CT parameters used for testing were: bone kernel H70h (sharp), slice thickness 0.70 mm, and image size of every axial CT slice 512 × 512 pixels, which, with variable reconstruction diameter, gave the axial voxel size range 0.45 × 0.45 mm to 0.90 × 0.90 mm. The Medinria imaging software was used for the visualization and manual localization of spherical fiducials and the surgery target planning. In our experiments, manual localization is conducted by skilled operators and compared with the localization algorithm using the methodology described below.

The transformation that maps the rigid body points between the image space and the physical space in real applications is considered to be imperfect and should contain certain errors. To measure the accuracy of the proposed localization algorithm we applied the theory of the medical image registration error introduced by Maurer, Jr., *et al.* [28] and Fitzpatrick *et al.* [29]. Fiducial registration error (FRE) is an error in aligning the corresponding fiducials after registration. FRE is defined as the root mean square distance between two sets of n matching fiducials after registration:

$$FRE^2 = \frac{\sum_{j=1}^{n} \left\| q_j - T(p_j) \right\|^2}{n}, \tag{1}$$

with q_j being the position of a single fiducial in the image space, and p_j being the exact position of a fiducial in the physical space. T is the rigid body transformation between the two sets. Fiducial localization error (FLE) is defined as the Euclidean distance between the true and the measured distance of the fiducial location. According to the aforementioned theory and a more recent study [30], if the ground truth measurement is available, FLE can be estimated based of N number of fiducials and FRE as:

$$FLE^2_{GT} = \frac{N}{N-2} FRE^2 \tag{2}$$

Intra-modal FLE estimation is based on two or more different CT scans of the same set of fiducials and it can be calculated as:

$$FLE^2_{IMAGE} = \frac{1}{2}\frac{N}{N-2} FRE^2, \tag{3}$$

for two different CT scans, or as:

$$FLE^2_{IMAGE} = \frac{N}{2M(N-2)} \sum_{m=1}^{M} FRE^2_m, \tag{4}$$

for more than two scans. M is the number of different registrations and FRE_m is the FRE of the m-th registration. In clinical application, the positioning accuracy of the targeted points is the most significant measure. Target registration error (TRE) is defined as the distance between the planned image target location and the physical target location after registration. Targeted points in neurosurgery are inside the brain and usually cannot be measured, so TRE can be estimated as the error in a given position r that may be caused by FLE. Assuming an isotropic error distribution of FLE, TRE is equal to:

$$TRE^2(r) \approx \frac{FLE^2}{N}\left(1 + \frac{\sum_{k=1}^{3} \frac{d_k^2}{f_k^2}}{3}\right), \tag{5}$$

with N being the number of fiducials, d_k the minimal distance of r from the k-th principal axis, and f_k the RMS distance of the fiducials from the k-th axis. It should be noted that even though equations (2-4) and (5) are found to be a reliable estimates of FLE and TRE [31], there are cases in which FRE does not approach the FLE as the number of fiducials increases and TRE from (5) is uncorrelated with the true TRE [32]. In [33] it is shown that for a single clinical case FRE and TRE are uncorrelated but equations (2-4) can be used to estimate mean value of FLE from FRE based on many measurements. From FLE, TRE can be estimated for that specific fiducial configuration and target position. To achieve reliable results we conducted a number of measurements with the same fiducial marker configuration found in both test phantoms and we inserted target points in the second test phantom for the purpose of evaluating the measurement results and applicability of the selected FLE estimation methods.

IV. AUTOMATIC LOCALIZATION IN CT IMAGES

Hypothetical planes that transect the human body in order to locate points of interest are axial (horizontal), sagittal (lateral), and coronal (frontal) plane. Reconstructed CT 3D volume is composed of a number of 2D slices from the axial plane. The 3D space between every two slices is the estimation of the intensity of the two original slices. Assuming that the highest degree of accuracy of the scan is found in the CT image slice itself, we first search for the potential spherical fiducials in the 2D axial slices. To confirm the found spheres and to calculate their centres, we additionally use the reconstructed sagittal 2D image slices. The main steps of the localization algorithm are shown in Fig. 3.

A. INTENSITY-BASED IMAGE FILTRATION

The pre-processing step in the automatic localization algorithm includes the intensity-based filtration of voxels. The fiducial marker consists of an X-shaped aluminium base with four steel pins (NDI - Northern Digital Inc., Ontario Canada). The outer geometry of steel pins fits the inner part of each of the four retro-reflective spherical fiducials. The tip of each steel pin is located around the geometrical centre of each spherical fiducial. The spherical fiducial is made of a homogeneous polymer and coated with a thin layer of fine-grained retro-reflective pearls. Both materials have the Hounsfield value similar to that of certain parts of the human anatomy and cannot be filtered by their intensity values. The radio-

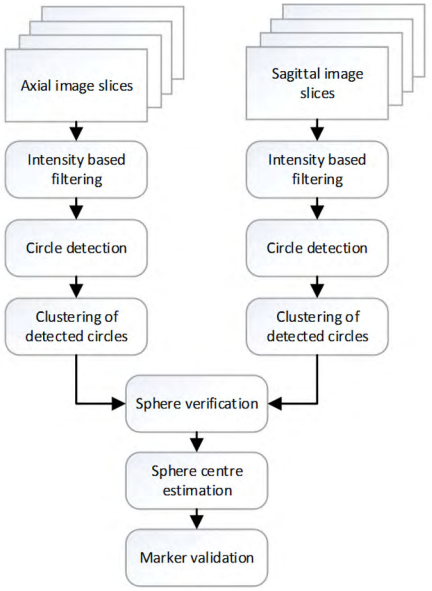

FIGURE 3. Automated localization algorithm flowchart.

density of the steel pins is very high and their intensity on the CT scans is saturated to +3071. In our CT scans, each voxel is stored as a 12-bit value in the range [−1024, 3071]. Binary threshold with a value of 3070 is used to convert each slice to a binary representation where all voxel intensities higher than 3070 are set to 1 and all other voxels are set to 0. Two binary morphological operators are further applied to each binarized slice representation. First, morphological closing (dilation followed by erosion) is performed, followed by the morphological shrink operator which removes pixels so that objects without holes shrink to a point while preserving the Euler number. After these steps, only slices where four steel pins and the titanium bone screw are located are segmented in such a way that they contain voxels with non-zero values. We generate a cubic (3D) ROI mask centred on all non-zero voxels. The side length of each ROI is equal to a 30% enlarged diameter of a spherical fiducial. The 30% enlargement is used as a safety factor so that each ROI is geometrically guaranteed to contain one whole spherical fiducial. In some cases, false positive results, i.e. false positive ROIs, are identified in the area of the patient's teeth because of dental fillings. As they are eliminated with the clustering algorithm, the only effect of the false positive results is the prolongation of the total computational time needed to search all the generated ROIs for circular objects, i.e. cross sections of spherical fiducials.

B. CIRCLE DETECTION

Regardless of the orientation, a cross section of any sphere is a circle. Based on that fact, we use a circle detection algorithm in the filtered axial and sagittal images to find all potential circles. The CHT-based algorithm was used for finding circles in images because of its robustness in the presence of noise, occlusion, and varying intensity [34]. Each circle in an image is found based on the known parameters of the retro-reflective spheres: radius span (r), algorithm threshold (Tr), and circle polarity (Pl). The radius span ranges from 50% to 120% of the nominal sphere radius. The circle polarity is set to light since the background of the CT images is dark and spheres are perceived as white.

TABLE 1. Algorithm for Circle detection.

Input: A_n and S_m are sets of axial and sagittal images **Output:** CCA and CCS are accumulated arrays of circles data with x and y as centre pixel coordinates, sl as slice number and r as radius		
1	**for each** A_n	//with n being axial number of images
2	**for each** C_p	//p is a number of potential circles in A_n
3	**If** $C_p == 1$ **then**	//according to (6)
4	CCA ← $[C_{px}, C_{py}, C_{psl}, C_{pr}]$	//append matrix row with circle centre information
5	**for each** S_m	//with m being axial number of images
6	**for each** C_p	//p is a number of potential circles in S_m
7	**If** $C_p == 1$ **then**	//according to (6)
8	CCS ← $[C_{px}, C_{py}, C_{psl}, C_{pr}]$	//append matrix row with circle centre information

$$C = f(r, Tr, Pl) \tag{6}$$

Based on the set system parameters used in (6), if a circle is valid, a non-zero binary value is assigned accordingly.

Given the pseudocode in Table 1, the C_{px}, C_{py}, C_{psl} denote the horizontal position, the vertical position, and the slice number, respectively, and C_{pr} denotes the radius of the C_p circle. The transformation from the image to the Cartesian coordinates (metric values) is carried out based on the CT scan metadata.

C. CIRCLE CLUSTERING AND SPHERE VERIFICATION

Potential spheres in the Cartesian space are segmented using the developed iterative clustering method. Clusters of circles are located from the circle centre axial (CCA) and circle centre sagittal (CCS) matrices. Low threshold setting used in the circle detection algorithm leads to the retrieval of false positive results, i.e. circles that are not part of spherical fiducials. False positive detections in regions around the marker frame and the patient's teeth are handled with the Euclidian distance filtering and bidirectional sphere verification. The first circles in the CCA and in the CCS matrix are designated as the first cluster. Euclidian distance filtering is used in both the 3D space and the 2D slice space to determine whether the next circle centre is part of any existing cluster. If not, a circle is labelled as the origin of a new cluster. This procedure is repeated for every circle centre. After all the circles have been processed, every cluster centroid CT_i is determined from the coordinates of all the n numbers of its members in the i-th cluster:

$$CT_i = \left[\frac{\sum_{j=1}^{n} x_j}{n}, \frac{\sum_{j=1}^{n} y_j}{n}, \frac{\sum_{j=1}^{n} z_j}{n} \right] \tag{7}$$

The clustering process described previously is repeated in two iterations to ensure that most of the circles are designated to their correct clusters. In the two iterations, the centroids of the real clusters converge to the centre of their sphere and the false circle readings are excluded from those clusters.

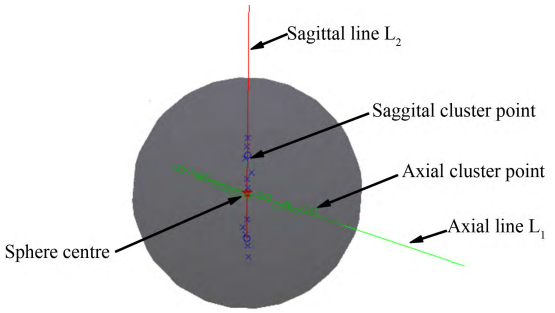

FIGURE 4. Visualization of the Linefit data.

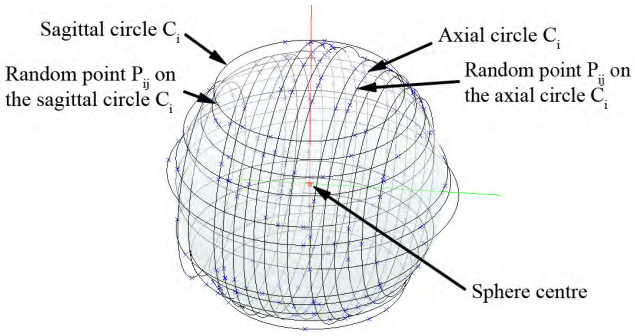

FIGURE 5. Visualization of the Spherefit data.

Finally, spheres are verified with bidirectional cluster proximity and cluster size. The minimal cluster size is set to three circles. Bidirectional cluster proximity denotes the validation of minimal predetermined distance between any two cluster centroids CT_i derived from the CCA and CCS matrices. Sphere centres are estimated with two different methods conveniently called Linefit and Spherefit:

1) RANSAC LINEFIT

For the estimation of sphere centre, the Random Sample Consensus (RANSAC) method [35] was implemented to fit the verified sphere cluster points from the axial and sagittal planes to their respective lines L_1 and L_2. Sphere cluster points are all the circle centres in the cluster that are used for the RANSAC line fitting. The advantage of RANSAC over other fitting methods such as the least squares fitting technique is that only the inlier points are used for the fitting of data. If a certain point in a data set differs, it is treated as an outlier. Minimal distance d between two estimated lines L_1 and L_2 from the axial and sagittal clusters is calculated from two closest points P and Q:

$$d\,(L_1, L_2) = _{P\in L_1} min_{Q\in L_2} d(P, Q) \tag{8}$$

The midpoint of the $\overline{PQ}$ line is the calculated sphere centre shown in Fig. 4.

2) SPHEREFIT

The second method used for the estimation of sphere centres is Spherefit. As shown in [36], a set of points is used for fitting algebraic surfaces using the direct least square method. Since this method is dimension-independent, it is suitable for sphere fitting. The data associated with the verified spheres contains circle centres with radii and all the detected circles that should lie on a spherical surface as shown in Fig. 5. Four random points P_{ij} (for j=1, 2, 3, 4) are generated from every circle C_i that is a part of the verified sphere:

$$C_i[x_i, y_i, z_i, r_i, rand(\alpha_{ij})] \rightarrow P_{ij}[x_{ij}, y_{ij}, z_{ij}] \tag{9}$$

Every P_{ij} is used as a point set for the calculation of the sphere centre.

The difference between the Spherefit and the RANSAC Linefit is that in the former all the data is used in the direct least square method for sphere centre calculation.

D. MARKER VERIFICATION

In the final step of the procedure, the distances between all spherical fiducials are compared to the known geometry of the fiducial marker. If the Euclidean distances between the calculated sphere centres are in the range $\pm e$ (allowed error) of the known nominal marker distances, the marker position is validated.

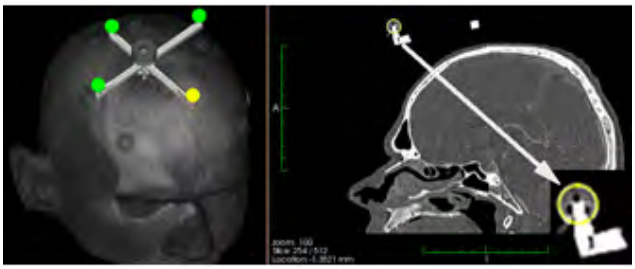

FIGURE 6. Visualization of a localized fiducial marker and a fiducial sphere.

Four verified fiducial points on the marker are automatically saved as an initial version of the preoperative plan. The saved plan is uploaded to the visualization software and the localized marker is shown to the operator or neurosurgeon. Visualization of the fiducial maker in the 3D and the sagittal view of one of the localized spherical fiducials are shown in Fig. 6.

V. CLINICAL TRIALS AND MEASUREMENTS

The purpose of measurements is to compare the accuracy, reliability, and speed of the human operators and the developed automatic localization algorithm. For the experiment, we acquired CT images of twelve patients with mounted fiducial markers and eight CT images of the two test phantoms shown in Fig. 2. Four scans were taken of the patients with the bone-attached fiducial marker that was mounted for the purpose of clinical testing of the complete RONNA system. All the other patients were scanned with the fiducial marker that was adhesively attached to their skin. Fig. 7 shows the robotic localization procedure of the fiducial marker during clinical trials.

Intra-modal and GT localization and registration accuracies were derived from five CT scans of the first test phantom with the same fiducial marker. The second test phantom was

FIGURE 7. Robot localization of the patient.

TABLE 2. Phantom ground truth fle estimation.

Image set number	FLE_{GT}		
	Human operators	Linefit	Spherefit
1	0.2956	0.0986	0.1030
2	0.3043	0.1627	0.0799
3	0.2243	0.0678	0.1042
4	0.3558	0.2354	0.2307
5	0.4146	0.2780	0.2907
MEAN FLE_{GT}	**0.3189**	**0.1685**	**0.1617**

scanned three times with a CT scanner. Scans of the test phantoms were taken on the same scanner with a different orientation for each scan. The GT was obtained by measuring the test phantoms on the CMM in the Croatian national laboratory for precise measurements of length. For comparison, the fiducial marker was localized in the image space by four skilled human operators and two previously described automated methods. FRE and FLE_{GT} were calculated using (1) and (2).

The mean FLE_{GT} for all human operators was 0.3189 mm, for Linefit 0.1685 mm, and for Spherefit 0.1617 mm, as shown in Table 2. Both the Linefit and the Spherefit centre estimation method showed smaller FLEs than any human operator individually in all CT scans. The lowest FLE values were obtained with the Spherefit method.

Intra-modal approximation of the FLE_{IMAGE} is calculated using (4) for $m=1\div10$ registrations derived from the same set of 5 phantom CT scans. The results are given in Table 3. The intra-modal approximation confirmed the GT results except for the estimated error values which were higher. FLE_{IMAGE} for human operators was 0.4698 mm, for Linefit 0.2604 mm, and for Spherefit 0.2541 mm.

TABLE 3. Phantom intra-modal fle estimation.

Registration number	FRE		
	Human operators	Linefit	Spherefit
1	0.3605	0.1748	0.1218
2	0.4075	0.0638	0.0731
3	0.4047	0.2018	0.2125
4	0.4021	0.2857	0.2785
5	0.4222	0.1327	0.1300
6	0.4165	0.3568	0.2506
7	0.5543	0.1466	0.2508
8	0.3423	0.2458	0.1798
9	0.5421	0.2470	0.3310
10	0.6523	0.4830	0.4673
MEAN FRE	**0.4504**	**0.2338**	**0.2295**
FLE_{IMAGE}	**0.4698**	**0.2604**	**0.2541**

From the patient CT scans, an additional intra-modal FLE_{IMAGE} approximation was calculated for a total of M=66 registrations. Patient scans were made with two almost identical fiducial markers and the fiducial spheres were changed after every operation. Since the identical fiducial set was not used due to interchangeable markers and spheres, we could not reliably estimate the intra-modal FLE. Hence, the calculated FLE_{IMAGE} from the patient CT scans was used only as confirmation of the results measured with the test phantom. The calculated FLE_{IMAGE} from the patient scans showed the same ranking and confirmed the measurements with the test phantom. Considering the calculated test phantom FLE_{GT} and the patient and the test phantom FLE_{IMAGE}, the Spherefit method has provided the best accuracy.

The second test phantom was used to measure the combined TRE and FLE and assess which FLE estimation type is the more appropriate measure for TRE estimation in our case. The fiducial spheres on the fiducial marker and target points were localised with the CMM and the localisation algorithm. After all the point coordinates were transformed into the coordinate system of the fiducial marker, the positioning error was calculated as a Euclidean distance between matching points. It should be noted that TRE estimation considers ideal target points which is not the case when we are comparing both fiducial points and target points localised in the CMM and the CT scans. Hence, because the target points are localised with the localization algorithm the TRE cannot be measured directly and the magnitude of the mean absolute error should be comparable with the sum of the TRE from fiducial marker registration and the localization error from the individual target points. Coordinates of 48 points localised from three CT scans were compared with CMM measurements. Mean absolute positioning error was 0.5431 mm for Linefit and

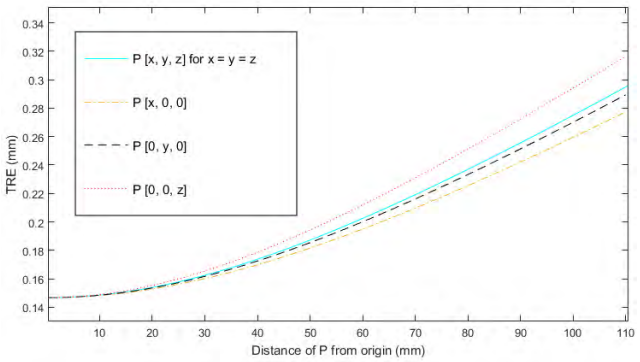

FIGURE 8. Spherefit TRE depending on different point P coordinates.

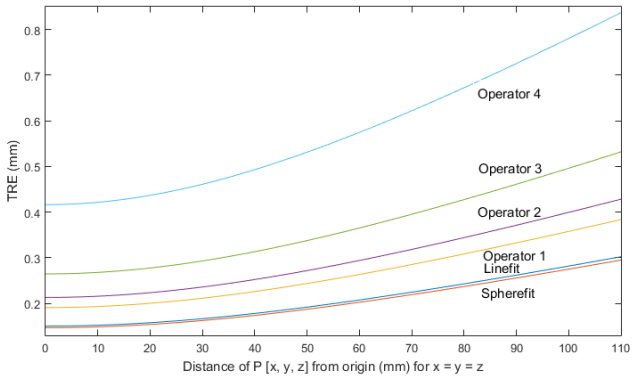

FIGURE 9. TREs in localization committed by operators and algorithms localizations for FLE_{IMAGE}.

0.5769 mm for Spherefit. RMS error was 0.4191 mm for Linefit and 0.4551 mm for Spherefit. Similarly to the results from the first test phantom, the second test phantom's mean FLE_{GT} was 0.1852 mm for Linefit and 0.1545 mm for Spherefit. FLE_{IMAGE} was 0.3406 mm for Linefit and 0.2738 mm for Spherefit. TRE estimation is calculated using (5) as a function of the second test phantom's FLE_{GT} and FLE_{IMAGE}, the fiducial marker configuration, and all the target points in the coordinate system of the fiducial marker. Average TRE for all target points is equal to 0.1841 mm based on 0.1545 mm Spherefit FLE_{GT} and 0.3263 mm based on 0.2738 mm Spherefit FLE_{IMAGE}. Target points average distance from the coordinate system origin is equal to 108.2037 mm. From the measured and the calculated values, it is observed that the values for FLE_{IMAGE} and the resulting TRE demonstrate the sum of 0.6001 mm which is a good match with the mean absolute positioning error of 0.5769 mm. Based on previous observation it was concluded that intra-modal FLE approximation is a more reliable measure for our case.

The spatial arrangement of the fiducial points on the marker causes the error estimation to slightly differ depending on the location of the target point in the marker coordinate system. Fig. 8 shows the TRE estimated from the first phantom's Spherefit FLE_{IMAGE} for the target located in point P [x, y, z] of the marker coordinate system. If the estimation of TRE is considered for a point P with the same distance from all the principal axes, the registration accuracy obtained with the localization algorithm is improved by 45.91% in comparison with the average human operator. Fig. 9 shows TREs in localization committed by operators and algorithms localizations.

The reliability and processing time of the localization algorithm are confirmed from the CT scans of twelve different patients and eight CT scans of the two test phantoms. All 116 fiducial spheres on the patient and phantom scans were successfully located and the fiducial marker configuration was validated in 100% of the cases. The average localization time of the human operator was 191.5 sec. The average localization time of the localization algorithm running on the i7-6700HQ CPU at 2.60GHz with 12GB RAM was 28.8 sec. In comparison with human operators, the localization algorithm reduces the time of the preoperative phase of marker localization by 84.96 %.

VI. CONCLUSION AND FUTURE WORK

The developed localization algorithm uses CT scan data for localizing spherical fiducials. A RONNA marker is composed of four spherical fiducials which are used for calculating the reference position of a patient in relation to planned surgery targets. Based on the measurements done in clinical conditions on the patients and test phantoms, the localization algorithm has shown a considerably higher degree of accuracy and higher speed in comparison with human operators. Reliability in terms of successful localization of the fiducial marker has been 100% in the twenty tested cases. The use of the localization algorithm reduces the imaging and the registration error significantly. In manual localization, operators have to visually determine the centre of every spherical fiducial in the exact order as the coordinate system of the marker has been defined. After the implementation of the automatic localization algorithm, the human operators and medical personnel reported less stress during the preoperative planning phase of the surgery. In the cases when the patient's CT scan is taken just before the surgical procedure, the overall duration of the surgery is reduced by the average of 162.7 sec.

In future work, we plan to develop an interconnected automatic system for the localization and registration of freely distributed non-invasive fiducial markers in the image space and the physical space. Non-invasive skin-attached markers have been reported to have a lower degree of registration accuracy than rigid bone-attached markers but, when used in a greater number, their accuracy improves [5]. The close loop registration system should include novel methods for image processing and marker localization in the image space, for global localization of a marker in the physical space, and for fine localization of the patient in the robot coordinate system. The system could be tested by means of a test phantom with a large number of fiducial points which would be used for measuring TRE. The preoperative surgery procedure could be considerably simplified if it did not include skull drilling and screw implantation. Based on the proposed system accuracy,

it would be decided in which procedures one can use the system.

ACKNOWLEDGEMENTS

The authors would like to thank the entire team from the hospital Dubrava (KB Dubrava), especially Prof. dr. sc. Darko Chudy, Domagoj Dlaka, dr. med, and dr.sc. Ana Hrkać-Pustahija for the tremendous help in the clinical studies and procedures. Authors would also like to thank dr. sc. Marko Katić from the Faculty of Mechanical Engineering and Naval Architecture, University of Zagreb, for measuring the test phantom on the CMM.

REFERENCES

[1] K. Cleary and T. M. Peters, "Image-guided interventions: Technology review and clinical applications," *Annu. Rev. Biomed. Eng.*, vol. 12, no. 1, pp. 119–142, Jul. 2010.

[2] P. P. Vaghasiya and P. K. Gautam, "Image registration techniques: A review," *Int. J. Eng. Comput. Sci.*, vol. 4, no. 2, pp. 10489–10492, Feb. 2015.

[3] J. V. Hajnal, D. J. Hawkes, and D. L. G. Hill, Eds., *Medical Image Registration*. Boca Raton, FL, USA: CRC Press, 2001.

[4] J. B.A. Maintz and M. A. Viergever, "A survey of medical image registration," *Med. Image Anal.*, vol. 2.1, no. 1, pp. 1–36, Mar. 1998.

[5] R. Steinmeier, J. Rachinger, M. Kaus, O. Ganslandt, W. Huk, and R. Fahlbusch, "Factors influencing the application accuracy of neuronavigation systems," *Stereotact. Funct. Neurosurg.*, vol. 75, no. 4, pp. 188–202, 2000.

[6] S. Poggi, S. Pallotta, S. Russo, P. Gallina, A. Torresin, and M. Bucciolini, "Neuronavigation accuracy dependence on CT and MR imaging parameters: A phantom-based study," *Phys. Med. Biol.*, vol. 48, no. 14, p. 2199, 2003.

[7] P. Markelj, D. Tomaževic, B. Likar, and F. Pernuš, "A review of 3D/2D registration methods for image-guided interventions," *Med. Image Anal.*, vol. 16, no. 3, pp. 642–661, 2012.

[8] R. Balachandran *et al.*, "Clinical testing of an alternate method of inserting bone-implanted fiducial markers," *Int. J. Comput. Assist. Radiol. Surg.*, vol. 9, no. 5, pp. 913–920, Sep. 2014.

[9] J. Mitchell, R. F. Labadie, and J. M. Fitzpatrick, "Design of a novel device to provide assured seating of bone implanted fiducial markers," *J. Med. Devices*, vol. 4, no. 2, p. 25002, 2010.

[10] C. R. Mascott, J.-C. Sol, P. Bousquet, J. Lagarrigue, Y. Lazorthes, and V. Lauwers-Cances, "Quantification of true *in vivo* (application) accuracy in cranial image-guided surgery: Influence of mode of patient registration," *Oper. Neurosurg.*, vol. 59, no. 1, pp. ONS-146–ONS-156, Jul. 2006.

[11] J. A. Smith, J. Jivraj, R. Wong, and V. Yang, "30 years of neurosurgical robots: Review and trends for manipulators and associated navigational systems," *Ann. Biomed. Eng.*, vol. 44, no. 4, pp. 836–846, Apr. 2016.

[12] P. Gomes, "Surgical robotics: Reviewing the past, analysing the present, imagining the future," *Robot. Comput.-Integr. Manuf.*, vol. 27, no. 2, pp. 261–266, Apr. 2011.

[13] B. Jerbić, G. Nikolić, D. Chudy, M. Švaco, and B. Šekoranja, "Robotic application in neurosurgery using intelligent visual and haptic interaction," *Int. J. Simul. Model.*, vol. 14, no. 1, pp. 71–84, 2015.

[14] M. Švaco, B. Šekoranja, F. Šuligoj, and B. Jerbić, "Calibration of an industrial robot using a stereo vision system," in *Proc. 24th DAAAM Int. Symp. Intell. Manuf. Autom.*, vol. 69. 2014, pp. 459–463. [Online]. Available: http://www.sciencedirect.com/science/article/pii/S1877705814002586

[15] F. Šuligoj, B. Jerbic, M. Švaco, B. Šekoranja, D. Mihalinec, and J. Vidakovic, "Medical applicability of a low-cost industrial robot arm guided with an optical tracking system," in *Proc. IEEE/RSJ Int. Conf. Intell. Robots Syst. (IROS)*, Sep. 2015, pp. 3785–3790.

[16] D. Á. Nagy, T. Haidegger, and Z. Yaniv, "A framework for semi-automatic fiducial localization in volumetric images," in *Augmented Environments for Computer-Assisted Interventions*. Boston, MA, USA: Springer, 2014, pp. 138–148.

[17] N. Gerber *et al.*, "High-accuracy patient-to-image registration for the facilitation of image-guided robotic microsurgery on the head," *IEEE Trans. Biomed. Eng.*, vol. 60, no. 4, pp. 960–968, Apr. 2013.

[18] M. Y. Wang, C. R. Maurer, J. M. Fitzpatrick, and R. J. Maciunas, "An automatic technique for finding and localizing externally attached markers in CT and MR volume images of the head," *IEEE Trans. Biomed. Eng.*, vol. 43, no. 6, pp. 627–637, Jun. 1996.

[19] Z. Yaniv, "Localizing spherical fiducials in C-arm based cone-beam CT," *Med. Phys.*, vol. 36, no. 11, pp. 4957–4966, 2009.

[20] Z. Yaniv, "Evaluation of spherical fiducial localization in C-arm cone-beam CT using patient data," *Med. Phys.*, vol. 37, no. 10, pp. 5298–5305, 2010.

[21] G. Fattori *et al.*, "Automated fiducial localization in ct images based on surface processing and geometrical prior knowledge for radiotherapy applications," *IEEE Trans. Biomed. Eng.*, vol. 59, no. 8, pp. 2191–2199, Aug. 2012.

[22] A. Isambert, G. Bonniaud, F. Lavielle, G. Malandain, and D. Lefkopoulos, "A phantom study of the accuracy of CT, MR and PET image registrations with a block matching-based algorithm," *Cancer/Radiothérapie*, vol. 12, no. 8, pp. 800–808, Dec. 2008.

[23] H. Suenaga *et al.*, "Vision-based markerless registration using stereo vision and an augmented reality surgical navigation system: A pilot study," *BMC Med. Imag.*, vol. 15, no. 1, p. 51, Dec. 2015.

[24] J. Gonzalez-Martinez *et al.*, "Robot-assisted stereotactic laser ablation in medically intractable epilepsy: Operative technique," *Neurosurgery*, vol. 10, pp. 167–173, Jun. 2014.

[25] M. Lefranc *et al.*, "The impact of the reference imaging modality, registration method and intraoperative flat-panel computed tomography on the accuracy of the ROSA stereotactic robot," *Stereotact. Funct. Neurosurg.*, vol. 92, no. 4, pp. 242–250, 2014.

[26] Q. H. Li, L. Zamorano, A. Pandya, R. Perez, J. Gong, and F. Diaz, "The application accuracy of the NeuroMate robot—A quantitative comparison with frameless and frame-based surgical localization systems," *Comput. Aided Surg.*, vol. 7, no. 2, pp. 90–98, Jan. 2002.

[27] D. von Langsdorff, P. Paquis, and D. Fontaine, "*In vivo* measurement of the frame-based application accuracy of the NeuroMate neurosurgical robot," *J. Neurosurg.*, vol. 122, no. 1, pp. 191–194, Jan. 2015.

[28] C. R. Maurer, Jr., J. J. McCrory, and J. M. Fitzpatrick, "Estimation of accuracy in localizing externally attached markers in multimodal volume head images," *Proc. SPIE*, vol. 1898, pp. 43–54, Sep. 1993.

[29] J. M. Fitzpatrick, J. B. West, and C. R. Maurer, Jr., "Predicting error in rigid-body point-based registration," *IEEE Trans. Med. Imag.*, vol. 17, no. 5, pp. 694–702, Oct. 1998.

[30] J.-P. Kobler, J. Díaz Díaz, J. M. Fitzpatrick, G. J. Lexow, O. Majdani, and T. Ortmaier, "Localization accuracy of sphere fiducials in computed tomography images," *Proc. SPIE*, vol. 9036, p. 90360Z, Mar. 2014.

[31] Z. Yaniv, "Rigid registration," in *Image Guided Interventions: Technology and Applications*, T. Peters and K. Cleary, Eds. New York, NY, USA: Springer, 2008, pp. 159–192.

[32] R. R. Shamir and L. Joskowicz, "Geometrical analysis of registration errors in point-based rigid-body registration using invariants," *Med. Image Anal.*, vol. 15, no. 1, pp. 85–95, Feb. 2011.

[33] J. M. Fitzpatrick, "Fiducial registration error and target registration error are uncorrelated," *Proc. SPIE*, vol. 7261, p. 726102, Mar. 2009.

[34] E. R. Davies, *Computer and Machine Vision: Theory, Algorithms, Practicalities*, 4th ed. Boston, MA, USA: Elsevier, 2012.

[35] M. A. Fischler and R. Bolles, "Random sample consensus: A paradigm for model fitting with applications to image analysis and automated cartography," *Commun. ACM*, vol. 24, no. 6, pp. 381–395, 1981.

[36] V. Pratt, "Direct least-squares fitting of algebraic surfaces," *ACM SIGGRAPH Comput. Graph.*, vol. 21, no. 4, pp. 145–152, 1987.

FILIP ŠULIGOJ received the B.Sc. and M.Sc. degrees in mechanical engineering from the Faculty of Mechanical Engineering and Naval Architecture, University of Zagreb, in 2008 and 2009, respectively, where he is currently pursuing the Ph.D. degree in robotics and automation. He is a Research and Teaching Assistant with the Faculty of Mechanical Engineering and Naval Architecture. His current research interests include the field of industrial and medical robotics, machine vision, and artificial intelligence methods.

MARKO ŠVACO received the B.Sc. and M.Sc. degrees in mechanical engineering, computer aided engineering with a specialization in intelligent assembly systems and the Ph.D. degree in robotics and automation from the Faculty of Mechanical Engineering and Naval Architecture, University of Zagreb (UNIZAG), Croatia, in 2008, 2009, and 2015, respectively. Since 2012, he has been an Associate with the Department of Neurosurgery, University Hospital Dubrava, Zagreb, Croatia. He is currently a Post-Doctoral Researcher and a Senior Teaching Assistant with the Faculty of Mechanical Engineering and Naval Architecture, UNIZAG. His current research interests include the field of industrial and medical robotics, artificial intelligence methods in robotics and computer vision.

BOJAN JERBIĆ received the B.Sc., M.Sc., and Ph.D. degrees from the Faculty of Mechanical Engineering and Naval Architecture, University of Zagreb, in 1983, 1987, and 1993, respectively. He is a Full Professor and the Head of the Chair of Manufacturing and Assembly System Planning. He is a member of the Scientific Board for Technology Development with the Croatian Academy of Science, the Croatian Robotics Society, and the Croatian Academy of Engineering - Department of Systems and Cybernetics. His main research interests include cognitive robotics, artificial intelligence, multiagent systems, new robotic applications, and medical robotics.

BOJAN ŠEKORANJA received the Diploma and Ph.D. degrees in mechanical engineering from the Faculty of Mechanical Engineering and Naval Architecture, University of Zagreb, in 2009 and 2015, respectively. He is currently a Post-Doctoral Research and Teaching Assistant with the Faculty of Mechanical Engineering and Naval Architecture. His current research interests include industrial and surgical robotics and human–robot interaction.

JOSIP VIDAKOVIĆ received the Diploma degree in mechanical engineering from the Faculty of Mechanical Engineering and Naval Architecture, University of Zagreb, in 2014, where he is currently pursuing the Ph.D. degree. He is a Research Assistant with the Faculty of Mechanical Engineering and Naval Architecture. His current research interests include the field of industrial and surgical robotics, artificial intelligence methods in robotics and computer vision.